RESEARCH ARTICLE

Gallic Acid Enhancement of Gold Nanoparticle Anticancer Activity in Cervical Cancer Cells

Jureerut Daduang[1]*, Adisak Palasap[1], Sakda Daduang[2], Patcharee Boonsiri[3], Prasit Suwannalert[4], Temduang Limpaiboon[1]

Abstract

Cervical cancer (CxCa) is the most common cancer in women and a prominent cause of cancer mortality worldwide. The primary cause of CxCa is human papillomavirus (HPV). Radiation therapy and chemotherapy have been used as standard treatments, but they have undesirable side effects for patients. It was reported that gallic acid has antioxidant, antimicrobial, and anticancer activities. Gold nanoparticles are currently being used in medicine as biosensors and drug delivery agents. This study aimed to develop a drug delivery agent using gold nanoparticles conjugated with gallic acid. The study was performed in uninfected (C33A) cervical cancer cells, cervical cancer cells infected with HPV type 16 (SiHa) or 18 (HeLa), and normal Vero kidney cells. The results showed that GA inhibited the proliferation of cancer cells by inducing apoptosis. To enhance the efficacy of this anticancer activity, 15-nm spherical gold nanoparticles (GNPs) were used to deliver GA to cancer cells. The GNPs-GA complex had a reduced ability compared to unmodified GA to inhibit the growth of CxCa cells. It was interesting that high-concentration (150 μM) GNPs-GA was not toxic to normal cells, whereas GA alone was cytotoxic. In conclusion, GNPs-GA could inhibit CxCa cell proliferation less efficiently than GA, but it was not cytotoxic to normal cells. Thus, gold nanoparticles have the potential to be used as phytochemical delivery agents for alternative cancer treatment to reduce the side effects of radiotherapy and chemotherapy.

Keywords: Cervical cancer cells - gallic acid - apoptosis - gold nanoparticles

Asian Pac J Cancer Prev, **16 (1)**, 169-174

Introduction

Worldwide, cervical cancer is the third most common cancer among women (Waggoner, 2003). Certain HPV types are carcinogenic in humans, and more than 99% of cervical cancers are associated with HPV infection (Monsonego et al., 2004). Radiotherapy is the treatment of choice for patients with locally advanced cervical carcinoma, and it results in a 70% progression-free survival rate (Rose, 2002). To increase local control rates, chemotherapeutic agents are being incorporated into treatment protocols. However, the success of chemotherapy in cervical cancer is hampered by drug resistance. Therefore, it is of critical importance that an effective treatment for cervical cancer be developed.

Phytochemical compounds can prevent, anti-inflammation (Rokayya et al., 2013) and inhibited several cancers such as breast cancer (Dilshad et al., 2012; Zhou et al., 2013) lung cancer (Ulasli et al., 2013). Gallic acid has been reported to prevent a number of diseases, including cancer (Lu et al., 2010; You et al., 2010; You and Park, 2010), cardiovascular disease (Patel and Goyal 2011), infection (Modi et al., 2013), and inflammation (Kroes et al., 1992). Gold nanoparticles (GNPs) have unique physicochemical properties, such as ultra-small size, a large surface area to mass ratio, high surface reactivity, the presence of surface plasmon resonance bands (Murphy et al., 2008), biocompatibility, and the ease of surface functionalization (Paciotti et al., 2006). This study examined the enhancement of gallic acid anticancer activity in both HPV-positive and HPV-negative cervical carcinoma cells by using gold nanoparticles as drug delivery agents. A putative mechanism of action for gallic acid and the induction of apoptosis by caspases 3/7, 8, and 9 was studied in these cell lines. The properties of GNPs may be utilized for targeted drug delivery in cancer, thus leading to increased efficacy for traditional chemotherapeutics.

Materials and Methods

Chemicals and reagents

Dulbecco's Modified Eagle's Medium-High Glucose (DMEM-HG), fetal bovine serum, penicillin-streptomycin,

*[1]Centre for Research and Development of Medical Diagnostic Laboratories, Faculty of Associated Medical Sciences, [2]Department of Biochemistry, Faculty of Science, [3]Department of Biochemistry, Faculty of Medicine, Khon Kaen University, Khon Kaen, [4]Department of Pathobiology, Faculty of Science, Mahidol University, Bangkok, Thailand *For correspondence: jurpoo@kku.ac.th*

and trypsin-EDTA were obtained from Gibco BRL (Grand Island, NY). Gallic acid, neutral red, and HAuCl4 were obtained from Sigma-Aldrich Co., LLC (Missouri). The Caspase-Glo 3/7, 8, and 9 reagents were obtained from Promega (Madison). Lead staining solution, propylene, and uranyl acetate were purchased from Sigma-Aldrich Co., LLC (Missouri).

Synthesis and conjugation of gold nanoparticles (GNPs)

Synthesis of bare GNPs: The gold nanoparticles were fabricated by following the classical method introduced by Turkevich et al. (1951). A volume of 95 ml of 0.01% chloroauric acid ($HAuCl_4 4H_2O$) solution was refluxed, and 5 ml of 1% sodium citrate solution was added to the boiling solution. The reduction of gold ions by citrate ions was completed after five minutes. The solution was boiled for an additional 30 minutes and then cooled at room temperature. This method yields spherical particles with an average diameter of approximately 15 nm. The size and morphology of the gold nanoparticles were analyzed by transmission electron microscopy (TEM) using a field emission high-resolution transmission electron microscope operating at 200 kV (TECNAI G2 20 Model). For TEM analysis, GNPs samples were prepared by dropping them onto a carbon film copper grid (Electron Microscopy Sciences, Pennsylvania) and drying in the oven. The optical absorption spectra in the wavelength range 350-650 nm was also measured using a spectrometer (Magellan 7 spectrophotometer, TECAN).

Conjugation of gold nanoparticles with gallic acid: A 200-µl volume of gold nanoparticle solution was centrifuged at 12,000 rpm for 10 min, the supernatant was removed, and the remaining pellet was dissolved in 200 µl DMEM-HG complete media. Then, gallic acid was separately added to the nanoparticles to reach a final concentration of 70-150 µM. The mixtures were stirred in the cold room overnight. Finally, to wash away unbound gallic acid, gold nanoparticles were centrifuged at 12,000 rpm for 10 min. The supernatant was removed and retained to measure unbound gallic acid by high performance liquid chromatography (HPLC); the remaining pellets were resuspended in DMEM-HG complete media (200 µl) and immediately used for further biological assays.

Gold nano-conjugation evaluation: *i*) Measurement of GNPs-GA size by spectrophotometry. Surface plasmon resonance band measurement by UV-Vis spectroscopy (Magellan 7 spectrophotometer, TECAN) was used to detect the size change from bare GNPs to GNPs-GAs. The optical absorption spectra were observed in the wavelength range from 350-650 nm. *ii*) Measurement of the concentration of unbound gallic acid after GNPs-GA conjugation by high liquid performance chromatography (HPLC)

The percentage of GNPs-GA conjugation was indirectly determined by HPLC by measuring the unbound gallic acid concentration in the GNPs-GA supernatant. A 20-µl aliquot of the supernatant from the GNPs-GA conjugation step was injected into a Luna C18 15 cm x 3.0 mm HPLC column (Phenomenex, California). Gradient elution was conducted at a flow rate of 1.5 ml/min using methanol and 0.5% phosphoric acid at ratios of 5:95, 70:30, 90:10, and 5:95 at 0-17, 17-18, 18-20.5 and 20.5-25 min, respectively. The absorbance at 270 nm (UV 2479, Waters) was detected, and the peaks were analyzed by the Clarity program (Waters). A 150 µM gallic acid concentration was used as the standard. Mean peak areas of unbound GA in the supernatant were calculated by comparing with the gallic acid standard area.

Detection of GNPs-GA uptake in cervical cell lines: *i*) Preparation of resin-embedded cells. HeLa cells were seeded in 6-well plates in DMEM-HG media for 24 h. Next, GNPs-GA complexes with a final concentration of 120 µM gallic acid were added to the cells and incubated at 37°C with 5% CO_2 for 12 h. The cells were harvested by trypsinization, washed twice with cold phosphate buffer saline (PBS), and centrifuged at 1,800 rpm for 3 min at room temperature. The supernatant was discarded, and the cells were fixed with 2% glutaraldehyde overnight. Then, cells were washed 4 times with 1X PBS and post fixed with osmium tetraoxide (OsO_4) for 2 h. Finally, fixed cells were washed twice with 1X PBS for 15 min each, dehydrated by washing with ethyl alcohol at 30%, 50%, 70%, 80%, 90% for 10 min each, and washed three times each with 95% and 100% ethyl alcohol for 10 min. Propylene was then added for 10 min. The cells were embedded by using embedding solution and propylene at ratios of 1:3, 1:1, and 3:1 for 1 h and pure embedding solution for 48 h. *ii*) Embedded cell sectioning and staining for transmission electron microscopy (TEM). Embedded cells were cut into 70 nm sections with a microtome (Reichert Ultracut), placed on a copper grid, stained by uranyl acetate (0.5 g uranyl acetate with 10 ml distilled water) for 5 min, washed with distilled water, stained with lead staining solution (0.01 g with 10 ml distilled water) for 5 min, and finally washed with distilled water. The morphological characterization of the gold nanoparticle uptake in cells was performed by TEM.

Cell culture

HeLa (HPV-18-positive), SiHa (HPV-16-positive), and C33A (HPV-negative) cervical cancer cells and Vero (normal) kidney cells were plated in 25-cm^2 tissue culture flasks at 37°C with 5% CO_2 in DMEM-HG media supplemented with 10% fetal bovine serum and 1% penicillin-streptomycin (10,000 U/ml penicillin and 10 mg/ml streptomycin). Once the cells were approximately 80% confluent, they were trypsinized with 1 ml of 1X trypsin-EDTA, incubated at 37°C for 5 min, and centrifuged at 1,800 rpm for 2 min. The supernatant was removed, a 200-µl cell pellet was resuspended in 5 ml of DMEM-HG media, and these cells were considered to be mycoplasma-free cell lines.

Cell viability and IC_{50} determination

The neutral red (NR) assay was used for cell viability analysis. Cervical cancer and Vero cells ($4x10^3$) in 100 µl of DMEM-HG media were used for cell viability tests. Each cell line was seeded into different 96-well plates. The cell lines were incubated with final concentrations of gallic acid from 20-150 µM, and the NR assay was performed.

The cells were then washed carefully with 250 µl of pre-warmed phosphate-buffered saline (PBS). After removing the rinsing solution, the cells were incubated with 200 µl of NR media (99 ml of DMEM-HG plus 1 ml of pre-filtered 3.3 mg/ml NR) for 3h. The incubated cells were washed with 1X PBS and then lysed with 100 µl of NR desorb solution (absolute ethanol: glacial acetic acid : distilled water at a ratio of 50:1:49). The plates were shaken for 30 min, and absorbance was measured at 540 nm using a spectrophotometer (Rayto RT-2100C, Germany). Cisplatin (20 µg/ml) was used as a positive control, and untreated cells were used as a negative control. The 50% inhibitory concentration (IC_{50}) was determined by plotting the percentage of cell viability versus drug concentrations. In vitro growth inhibition assays for GNPs-GA complexes on cervical carcinoma cell lines and Vero cell lines were incubated with various final concentrations (20-150 µM) of gallic acid conjugated to GNPs at 37°C for 24 h, and the NR assay was performed following the same procedure. Each concentration of drug treatment was repeated in six wells for three independent experiments.

Apoptosis pathway analysis by caspase activity assay

The caspase activity assay was analyzed using a test kit (Promega). Cells ($4x10^3$) in 100 µl of media were seeded into different black 96-well plates. A final concentration of 60 µM gallic acid (a subtoxic dose) was added to the cell lines and incubated at 37°C for 12 h. The cells were incubated at room temperature and were then mixed with 100 µl of Caspase-Glo 3/7, 8, and 9 reagents per well of a black 96-well plate also containing a blank, a negative control and treated cells in culture media. The contents of the wells were gently mixed with a plate shaker at 300-500 rpm for 30 sec and incubated at room temperature for 1 h. The luminescent signal of each sample was read with a SpectraMax L Luminescence microplate reader (Devices LLC, California). The data were analyzed by using Soft Max® Pro software (Devices LLC, California).

Results

Measurement of conjugated gold nanoparticle size

The obtained bare GNPs were ruby red, indicating that nanoparticles were formed. The average diameter of these GNPs was approximately 15 nm, which was determined by selecting 100 GNPs randomly from a TEM photograph as shown in Figure 1.

Conjugation of gold nanoparticles with gallic acid

After gold particle nanoconjugation, the GNPs-GA formation was evaluated by surface plasmon resonance using a UV-visible spectrophotometer. As shown in Figure 2, GNPs have a maximum absorption of 525 nm, whereas GNPs-GA have shifted maximum absorption values of 560 nm. This finding indicates that the GNPs were conjugated with GA, which caused plasmon resonance spectral shifting.

Measurement of the concentration of unbound gallic acid after GNPs-GA conjugation by HPLC

To confirm gold nanoparticle synthesis by an indirect method, the supernatant that was discarded after the GNPs-GA conjugation step was tested for remnant unbound gallic acid by HPLC. Compared to the gallic acid standard retention time at 7.5 min, the supernatant had no peak at this retention time (Figure 3). The results show that GNPs-GA conjugation was complete.

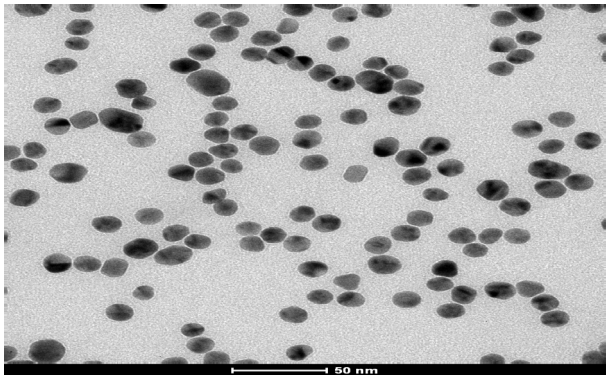

Figure 1. Transmission Electron Microscopy Image of GNPs at a Magnification of 100,000. The Scale Bar Denotes 50 nm. The Average Diameter of the GNPs is Approximately 15 nm

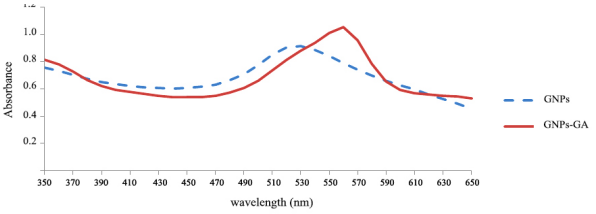

Figure 2. Surface Plasma Resonance Spectra of GNPs before and after Surface Conjugation with Gallic Acid (GNPs-GA) by UV-Visible Spectrophotometer Scanning in the Range from 350-650 nm

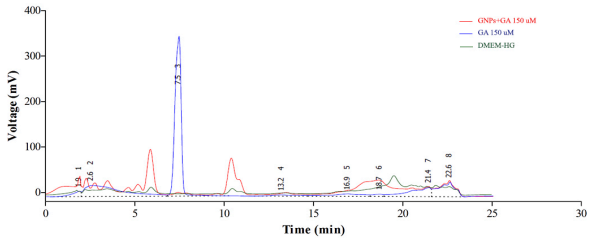

Figure 3. HPLC chromatogram of Gallic Acid Standard (blue line), the Supernatant that was Discarded after the GNP-GA Conjugation Step (red line), and the Negative Control DMEM-HG (green line)

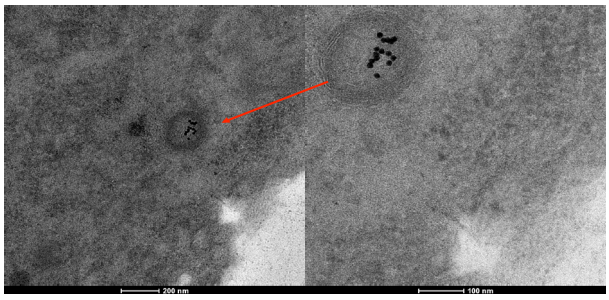

Figure 4. TEM image of HeLa Cells Incubated with GNPs-GA in Media after 12 h; A) GNPs-GA in Vacuoles and B) GNPs-GA in the Cytoplasm

Detection of GNPs-GA uptake in cervical cell lines

To address the intracellular distribution/location of nanoparticles, HeLa cells were treated with GNPs-GA and embedded into resin. The 70-nm thick cell sections were stained and visualized by TEM. As shown in Figure 4, GNPs-GA were internalized by endocytosis, and some dark spots were only observed in the cytoplasm.

Evaluation of the effects of GNPs-GA and unmodified GA on cervical cell lines

To evaluate the effects of GNPs-GA and unmodified GA on cervical cancer cell lines, the cytotoxicity test was performed by neutral red assay. Surprisingly, the cells treated with GNPs-GA had increased viability compared to cells treated with GA alone (Figure 5A). In Vero cells, GA-treated cells showed a dramatic decrease in cell viability (Figure 5B), whereas GNPs-GA had no effect on the percentage of viable cells even at high concentrations (90-150 μM; Figure 5A). Interestingly, this result indicated that high concentrations of GNPs-GA were cytotoxic to only certain cancer cell lines but not to normal cell lines.

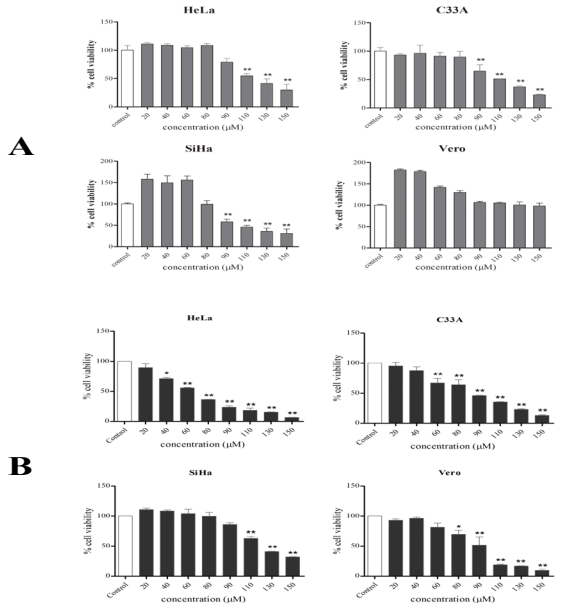

Figure 5. Cell viability of HeLa, C33A, SiHa, and Vero Cells Exposed to A) GNPs-GA and B) GA Alone for 24 h

Caspase assay measurement of apoptosis induction in cancer cells by gallic acid

The treatment of HeLa, SiHa, and C33A cervical cancer cell lines with gallic acid induced cellular morphological alterations consistent with the initiation of apoptosis. Thus, the caspase activity of HeLa, SiHa, and C33A cells was examined. As shown in Figure 6, treatment with gallic acid caused a considerable increase in caspase activation in all cancer cells. At the same concentration of gallic acid, HeLa cells had the highest caspase activity. The results showed that caspases 3/7, 8, and 9 were significantly more active in HeLa and SiHa cells treated with GNPs-GA compared to control treatments.

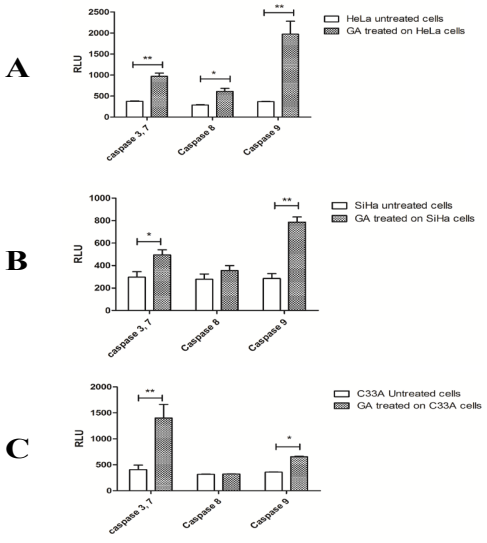

Figure 6. Caspase 3/7, 8, and 9 Activity in A) HeLa B) SiHa and C) C33A Cells Following Treatment with Gallic Acid at 60 μg/ml for 12 h. Data Represent the Mean Values±SD from Six Independent Experiments *p<0.05 and **p<0.01 Compared to the Control

Discussion

Gallic acid can inhibit tumor development by several mechanisms, such as the inhibition of metastasis (Ohno, Inoue et al., 2001); the suppression of angiogenesis (Liu et al., 2014); the induction of apoptosis and/or necrosis (You et al., 2010); the inhibition of cell viability, proliferation, invasion and tube formation (Lu, Jiang et al., 2010); and the inhibition of migration and invasion (Liao et al., 2012). In the present study, the effects of gallic acid were investigated in human cervical cell lines (HeLa, SiHa, and C33A). Differences in response to the agents were observed in the 3 cell lines. SiHa cells were the most resistant to gallic acid, and HeLa cells were the most sensitive. Palasap et al. (2014) also reported that the potency of gallic acid was greater in HeLa cells compared to other cervical cancer cell lines.

You et al. (2010) reported that GA-induced apoptosis in HeLa cells was accompanied by the slight down-regulation of Bcl-2 and the up-regulation of Bax, indicating that the mitochondrial release of cytochrome c can be controlled by the Bcl-2 family of proteins. Our study found that caspases 3/7, 8, and 9 were significantly more active in HeLa cells treated with gallic acid, which indicates the induction of apoptosis via intrinsic and extrinsic pathways. However, SiHa and C33A cells only showed increased caspase 8 levels, which reveals that gallic acid induced apoptosis via the intrinsic pathway. The HeLa and SiHa cells are infected with HPV, which results in p53 degradation (Kim et al., 2013). However, this study showed that gallic acid could induce the intrinsic pathway via extrinsic pathway II. In the extrinsic pathway II, active caspase 8 cleaves BID within the native complex on the mitochondrial membrane, which results in the formation of tBID. The cleavage of BID exposes the BH3 domain and may drive the dissociation of tBID from the caspase-8/BID complex. Then, tBID shifts to separate complexes on the mitochondrial membrane and interacts with BAK and/or BCL-XL to activate mitochondrial outer membrane

permeabilization (MOMP). Apoptogenic factors, such as cytochrome c and Smac/DIABLO, are released from the mitochondria, leading to the activation of effector caspases and cell death (Schug et al., 2011).

Several studies revealed that compounds conjugated with gold nanoparticles are more cytotoxic than the free compounds (Manju and Sreenivasan 2012; Eshghi et al., 2013; Sanchez et al., 2014). In this study, GNPs-GA exhibited less cytotoxicity than GA alone. However, at the same high concentrations, GNPs-GA were non-toxic to Vero (normal) cells and were only toxic to cervical cancer cells. In addition, the GNPs-GA distribution and location were monitored. GNPs-GA was observed only in the cytoplasm and was taken up into cells via endocytosis, similar to the report of Tsai et al. (2008). At low concentrations (20-80 μM), GNPs-GA can induce cell proliferation compared to control. The GNPs at a few concentrations can promote the cell proliferation of keratinocytes (Lu et al., 2010). However, at the same high concentrations, GNPs-GA was non-toxic to Vero (normal) cells and were toxic to cervical cancer cells. Several studies reported that the electrical properties of cancer cells, such as those of breast (Dobrzynska et al., 2013), human large intestine (Szachowicz et al., 2002) and human colorectal cancer (Dobrzynska et al., 2005), are different from those of normal cells. The uptake efficiency of the positively charged GNPs was greater than that of the neutral and negatively charged GNPs (Chithrani, 2010). The high uptake of positively charged NPs was explained using a theoretical model (Cho et al., 2009); positively charged GNPs should adhere to the negatively charged cell membranes and facilitate increased uptake into cells. Zhou et al. (2010) reported that tumor cells required supplements to proliferate (Zhou et al., 2010) and that tumor cells ingested GNPs-GA into the cytoplasm, resulting in reduced cell viability for cancer cells compared to normal cells. To enhance the efficacy of cancer therapy, GNPs-GA were combined with other techniques for cancer treatment such as photothermal therapy (Afifi et al., 2013), magnetic fields (Hayashi et al., 2013), and ultrasound (Lentacker et al., 2010).

In conclusion, high concentrations of gallic acid conjugated with gold nanoparticles are cytotoxic toward certain cancer cell lines but are safe for normal cell lines. To enhance the anticancer activity of gold nanoparticles in cervical cell lines, GNP surfaces can be functionalized by specific bioconjugation. This method will be useful for targeting a cancer biomarker for specific inspection or therapy. Further studies are needed to target cancer cells specifically and to translate these developments into targeted therapy in cervical cancer patients.

Acknowledgements

This work was supported by the Higher Education Research Promotion and National Research University Project of Thailand, Office of the Higher Education Commission, through the Health cluster (SHeP-GMS), Khon Kaen University and the Centre for Research and Development of Medical Diagnostic Laboratories, Faculty of Associated Medical Sciences, Khon Kaen University.

References

Afifi MM, El Sheikh SM, Abdelsalam MM, et al (2013). Therapeutic efficacy of plasmonic photothermal nanoparticles in hamster buccal pouch carcinoma. *Oral Surg Oral Med Oral Pathol Oral Radiol*, **115**, 743-51.

Chithrani DB (2010). Intracellular uptake, transport, and processing of gold nanostructures. *Mol Membr Biol*, **27**, 299-311.

Cho EC, Xie J, Wurm PA, et al (2009). Understanding the role of surface charges in cellular adsorption versus internalization by selectively removing gold nanoparticles on the cell surface with a I2/KI etchant. *Nano Lett*, **9**, 1080-4.

Dilshad A, Abulkhair O, Nemenqani D, Tamimi W (2012). Antiproliferative properties of methanolic extract of *Nigella sativa* against the MDA-MB-231 cancer cell line. *Asian Pac J Cancer Prev*, **13**, 5839-42.

Dobrzynska I, Skrzydlewska E and Figaszewski Z A (2013). Changes in electric properties of human breast cancer cells. *J Membr Biol*, **246**, 161-6.

Dobrzynska I, Szachowicz-Petelska B, Sulkowski S, Figaszewski Z (2005). Changes in electric charge and phospholipids composition in human colorectal cancer cells. *Mol Cell Biochem*, **276**, 113-9.

Eshghi H, Sazgarnia A, Rahimizadeh M, et al (2013). Protoporphyrin IX-gold nanoparticle conjugates as an efficient photosensitizer in cervical cancer therapy. *Photodiagnosis Photodyn Ther*, **10**, 304-312.

Hayashi K, Nakamura M, Sakamoto W, et al (2013). Superparamagnetic nanoparticle clusters for cancer theranostics combining magnetic resonance imaging and hyperthermia treatment. *Theranostics*, **3**, 366-376.

Kim MS, Bak Y, Park YS, et al (2013). Wogonin induces apoptosis by suppressing E6 and E7 expressions and activating intrinsic signaling pathways in HPV-16 cervical cancer cells. *Cell Biol Toxicol*, **29**, 259-272.

Kroes BH, van den Berg AJ, Quarles van Ufford HC, van Dijk H, Labadie RP (1992). Anti-inflammatory activity of gallic acid. *Planta Med*, **58**, 499-504.

Lentacker I, Geers B, Demeester J, De Smedt SC, Sanders NN (2010). Tumor cell killing efficiency of doxorubicin loaded microbubbles after ultrasound exposure. *J Control Release*, **148**, 113-4.

Liao CL, Lai KC, Huang AC, et al (2012). Gallic acid inhibits migration and invasion in human osteosarcoma U-2 OS cells through suppressing the matrix metalloproteinase-2/-9, protein kinase B (PKB) and PKC signaling pathways. *Food Chem Toxicol*, **50**, 1734-40.

Liu X, Huang N, Li H, et al (2014). Multidentate polyethylene glycol modified gold nanorods for in vivo near-infrared photothermal cancer therapy. *ACS App Mater*, **6**, 5657-68.

Lu S, Xia D, Huang G, et al (2010). Concentration effect of gold nanoparticles on proliferation of keratinocytes. *Colloids Surf B Biointerfaces*, **81**, 406-411.

Lu Y, Jiang F, Jiang H, et al (2010). Gallic acid suppresses cell viability, proliferation, invasion and angiogenesis in human glioma cells. *Eur J Pharmacol*, **641**, 102-107.

Manju S, Sreenivasan K (2012). Gold nanoparticles generated and stabilized by water soluble curcumin-polymer conjugate: blood compatibility evaluation and targeted drug delivery onto cancer cells. *J Colloid Interface Sci*, **368**, 144-151.

Modi M, Goel T, Das T, et al (2013). Ellagic acid & gallic acid from Lagerstroemia speciosa L. inhibit HIV-1 infection through inhibition of HIV-1 protease & reverse transcriptase activity. *Indian J Med Res*, **137**, 540-8.

Monsonego J, Bosch FX, Coursaget P, et al (2004). Cervical cancer control, priorities and new directions. *Int J Cancer*,

108, 329-33.
Murphy CJ, Gole AM, Stone JW, et al (2008). Gold nanoparticles in biology: beyond toxicity to cellular imaging. *Acc Chem Res*, **41**, 1721-30.
Ohno T, Inoue M and Ogihara Y (2001). Cytotoxic activity of gallic acid against liver metastasis of mastocytoma cells P-815. *Anticancer Res*, **21**, 3875-80.
Paciotti GF, Kingston DG I and Tamarkin L (2006). Colloidal gold nanoparticles: a novel nanoparticle platform for developing multifunctional tumor-targeted drug delivery vectors. *Drug Development Research*, **67**, 47-54.
Palasap A, Limpaiboon T, Boonsiri P, et al (2014). The cytotoxic effect of phytophenolics form *Caesalpinia mimosoides* Lamk on cervical carcinoma cell lines through apoptotic pathway. *Asian Pac J Cancer Prev*, **15**, 449-454.
Patel SS, Goyal RK (2011). Cardioprotective effects of gallic acid in diabetes-induced myocardial dysfunction in rats. *Pharmacognosy Res*, **3**, 239-245.
Rokayya S, Li CJ, Zhao Y, Li Y, Sun CH (2013). Cabbage (*Brassica oleracea* L. var. capitata) phytochemicals with antioxidant and anti-inflammatory potential. *Asian Pac J Cancer Prev*, **14**, 6657-62.
Rose PG (2002). Chemoradiotherapy for cervical cancer. *Eur J Cancer*, **38**, 270-278.
Sanchez-Paradinas S, Perez-Andres M, Almendral-Parra MJ, et al (2014). Enhanced cytotoxic activity of bile acid cisplatin derivatives by conjugation with gold nanoparticles. *J Inorg Biochem*, **131**, 8-11.
Schug ZT, Gonzalvez F, Houtkooper RH, Vaz FM, Gottlieb E (2011). BID is cleaved by caspase-8 within a native complex on the mitochondrial membrane. *Cell Death Differ*, **18**, 538-48.
Szachowicz-Petelska B, Dobrzynska I, Figaszewski Z, Sulkowski S (2002). Changes in physico-chemical properties of human large intestine tumour cells membrane. *Mol Cell Biochem*, **238**, 41-47.
Tsai SW, Chen YY and Liaw JW (2008). Compound cellular imaging of laser scanning confocal microscopy by using gold nanoparticles and dyes. *Sensors*, **8**, 2306-2316.
Turkevich J, Stevenson PC, Hillier J (1951). A study of the nucleation and growth processes in the synthesis of colloidal gold. *Discuss Faraday Soc*, **11**, 55-75.
Ulasli SS, Celik S, Gunay E, et al (2013). Anticancer effects of thymoquinone, caffeic acid phenethyl ester and resveratrol on A549 non-small cell lung cancer cells exposed to benzo(a) pyrene. *Asian Pac J Cancer Prev*, **14**, 6159-64.
Waggoner SE (2003). Cervical cancer. *Lancet*, **361**, 2217-25.
You BR, Moon HJ, Han YH, Park WH (2010). Gallic acid inhibits the growth of HeLa cervical cancer cells via apoptosis and/or necrosis. *Food Chem Toxicol*, **48**, 1334-1340.
You BR, Park WH (2010). Gallic acid-induced lung cancer cell death is related to glutathione depletion as well as reactive oxygen species increase. *Toxicol In Vitro*, **24**, 1356-62.
Zhou W, Shao J, Jin Q, et al (2010). Zwitterionic phosphorylcholine as a better ligand for gold nanorods cell uptake and selective photothermal ablation of cancer cells. *Chem Commun (Camb)*, **46**, 1479-81.